IEEE Open Journal of the Communications Society

Received XX Month, XXXX; revised XX Month, XXXX; accepted XX Month, XXXX; Date of publication XX Month, XXXX; date of current version XX Month, XXXX.

Digital Object Identifier 10.1109/OJCOMS.YEAR.NUMBER

On Symbol Error Performance of Probabilistic Shaping in Noise-Limited and Fading Channels

Tilahun Zerihun Gutema[1] ***(Graduate Student Member, IEEE),*** **Harald Haas[2]** ***(Fellow, IEEE),*** **and Wasiu O. Popoola[1]** ***(Senior Member, IEEE)***

[1]Institute for Digital Communications, School of Engineering, The University of Edinburgh, Edinburgh, EH9 3FD, United Kingdom
[2]The Technology and Innovation Centre, University of Strathclyde, 99 George Street, Glasgow, G1 1RD, United Kingdom

CORRESPONDING AUTHOR: Tilahun Zerihun Gutema (e-mail: tilahun.gutema@ed.ac.uk).

The work is funded by the European Union H2020-MSCA-ITN-2018 №: 814215 grant titled ENLIGHT'EM: European Training Network in Low-Energy Visible Light IoT Systems: https://enlightem.eu/.

ABSTRACT In this work, we present symbol error performance analysis of probabilistic shaping (PS) for wireless communications in noise-limited and fading channels. Two fading models considered are the Rayleigh and log-normal fading channels. The results are corroborated with simulation and compared with the conventional uniformly distributed input symbols. In all channel conditions, PS results in significant reductions in the SNR required to achieve a specific error probability compared to the conventional uniformly shaped symbols. For example, in a noise-limited channel, PS based quadrature amplitude modulation (QAM) signal results in SNR gains of 1.16 dB, 1.41 dB, and 1.52 dB compared to the uniformly distributed QAM symbols at equal entropy rates of 4, 6, and 8 bit/symbol and a symbol error ratio (SER) of 1×10^{-3}.

INDEX TERMS Probabilistic shaping (PS), error probability, wireless communication, Rayleigh fading, log-normal fading.

I. INTRODUCTION

ENHANCING spectral efficiency and optimising the use of available scarce resources are crucial requirements of any communication systems. Yet, in the conventional data transmission, in which each symbol (or constellation point) is transmitted with equal probability, the distribution of input symbols is not a perfect fit for the linear additive white Gaussian noise (AWGN) channel. Consequently, it does not allow for optimal utilisation of the channel capacity [1]. Moreover, in a wireless channel, the influence of fading and multipath propagation deteriorate the system performance [2].

The error probability of pulse-amplitude modulation (PAM) and quadrature amplitude modulation (QAM) in AWGN channels has been studied extensively [2]–[4]. Moreover, several works have also presented the performance of wireless communication systems in Rayleigh and log-normal fading conditions [5]–[7]. In [5], tight upper and lower bounds on the error probability of coded modulation schemes in Rayleigh fading channels are studied. The average error probability in fading channels for different modulation techniques has also been evaluated by approximating the sum of two exponential functions in [6]. For a multiple access cellular uplink network in Rayleigh fading, a tight upper bound symbol error probability is also derived in [7]. However, all these studies consider only uniformly distributed input symbols.

Optimising the distribution of source symbols through signal shaping is crucial for enhancing communication system performance. One shaping method that has garnered considerable attention is probabilistic shaping (PS). It involves adjusting the probabilities of occurrence of constellation points to create a Gaussian-like distribution [1], [8]. Thus, resulting in non-uniform distribution of data symbols. Therefore, by applying PS to QAM symbols, low-energy symbols are transmitted more frequently than high-energy symbols. This is realised by using a distribution matcher, such as a constant composition distribution matcher

This work is licensed under a Creative Commons Attribution 4.0 License. For more information, see https://creativecommons.org/licenses/by/4.0/

(CCDM), proposed in [9], which maps input information bits into non-equiprobable symbols with a Gaussian-like distribution. The Maxwell-Boltzmann distribution is commonly used to generate Gaussian-like signalling which has been shown theoretically to attain the ultimate shaping gain ($\pi e/6$ or 1.53 dB) [8], [10], [11]. PS is essentially an approach to trade energy efficiency for spectral efficiency.

PS has shown to be an optimum technique in optical fibre communications to achieve record-setting transmission rates and distances [1], [12]–[14], as well as in optical wireless communications [15]–[17]. Similarly, PS has been employed in wireless communications to maximise transmission capacity and improve system performance. For example, PS has contributed to a substantial improvement in transmission capacity and system performance for high-speed Terahertz photonic wireless communication systems in [18]–[20]. PS has also been applied to mitigate hardware distortions in [21]. Therefore, it is important to study the error performance of PS in wireless communication systems in the presence of fading. Related work in this domain include, designing PS with constellation rotation and component interleaving for diversity gain in [22].

In this paper, we study the theoretical symbol error performance of PS. For such a scheme, the maximum likelihood detection will not be applicable. Therefore, an optimum maximum a posteriori (MAP) detector is derived. The symbol error ratio (SER) of PS based uncoded QAM with modulation order, M, (PS-M-QAM) under Gaussian noise-limited condition is analysed, and analytical expressions are provided. The results are compared with the conventional uniformly distributed uncoded QAM symbols. We extend the PS approach to Rayleigh and log-normal fading channel conditions and derive expressions to estimate the PS performance in the presence of fading. The presented analysis is based on symbol error rate and therefore agnostic of the choice of bits-to-symbol distribution matcher. The findings from this study can be extended to investigate the PS bit error rate (BER). The BER of PS depends on the choice of distribution matcher used. Moreover, the distribution dematcher is sensitive to errors and it usually needs to be accompanied with forward error correction (FEC). That is, FEC encoding along with the PS distribution matcher in the transmitter and FEC decoder and distribution dematcher in the receiver. The order of shaping and coding processing steps in the transmitter and receiver is still an open and yet interesting research to investigate [12], [23].

We analyse the impact of a rate parameter, which is used to find an optimum probability mass function (PMF), on the entropy and the error performance of the system. We also compare the SNR gain using a rate parameter which provides an equal entropy between PS and uniformly distributed QAM symbols. In all cases, the theoretical results are verified with Monte Carlo simulations and show significant gains over the conventional uniformly distributed QAM symbols. For example, in a noise-limited channel, PS-16-QAM, PS-64-QAM, and PS-256-QAM with respective source entropy, H = {3.6, 5.4, 7.2} bit/symbol can provide SNR gains of about 2.12 dB, 2.89 dB, 3.45 dB compared to the conventional uniform 16-QAM, 64-QAM, 256-QAM at SER = 10^{-3}, respectively. Meanwhile, comparing at equal entropy, H = {4, 6, 8} bit/symbol between uniform 16-QAM, 64-QAM, and 256-QAM against higher order PS-M-QAM, PS QAM provides SNR gains of 1.16 dB, 1.41 dB, and 1.52 dB at the same SER. These results approach the ultimate shaping gain (1.53 dB) that can be achieved using a Gaussian distribution over uniform distribution at an equal entropy rate [8].

The rest of the paper is organised as follows: Section II presents a generation and detection of PS based symbols. In Section III, the error performance analysis of PS-QAM in an AWGN channel condition is presented. This is then extended to fading channel conditions in Section IV. Performance in log-normal fading condition is presented in subsection A while that of Rayleigh fading channel is presented in subsection B. Finally, conclusions are given in Section V.

II. GENERATION AND DETECTION OF PS SYMBOLS

In this section, the basics of generating PS based symbols using a Gaussian-like input distribution is presented and an optimum maximum a posteriori (MAP) detector is derived.

A. Generating PS Symbols

The constellation of an M-QAM can be considered as two orthogonal $\sqrt{M}$-PAM constellations which are chosen independently over a set comprising $x_m = \left\{2m - 1 - \sqrt{M}\right\}$, $m = 1, 2, \cdots, \sqrt{M}$. In PS-$M$-QAM, to maximise the channel capacity of a Gaussian channel, symbols are chosen from a Gaussian-like input distribution [8], [10]. The common approach is to use the input distribution from the family of Maxwell-Boltzmann distribution whose 1-dimensional form is represented as [14], [24]:

$$p_X\left(x_m\right) = \frac{1}{\sum_{j=1}^{\sqrt{M}} \mathrm{e}^{-\lambda|x_j|^2}} \mathrm{e}^{-\lambda|x_m|^2}, \tag{1}$$

with $\lambda \geq 0$ representing the rate parameter. It is used to search for the optimum PMF depending on the choice of entropy, $H = -\sum_{x_m \epsilon X} p_X\left(x_m\right) \log_2\left(p_X\left(x_m\right)\right)$ and average symbol energy, $\xi_{\mathrm{av}} = \sum_{x_m \epsilon X} \left|x_m\right|^2 p_X\left(x_m\right)$. Appendix A explains the relationship between the rate parameter, variance of a Gaussian distribution and illustrates how the Maxwell-Boltzmann distribution approximates it. For $\lambda = 0$, the distribution is uniform while it becomes Gaussian distribution with reduced variance as λ increases. The PMF of an M-QAM constellation is the product of the respective constituent PAM probabilities.

B. Detection of PS Symbols

The optimum detection scheme for PS is based on the MAP detector. This is because the detection needs to take the priori symbol distribution into account unlike the maximum

likelihood detector that does not [3]. In this section, the MAP detector for PS with Maxwell-Boltzmann distribution is discussed. The analysis is based on a one-dimensional M-PAM signal which can be easily extended to a two-dimensional QAM signal.

Consider an AWGN channel such that the received symbols over a symbol duration are defined as $Y = X+Z$, where X is the transmitted input symbols and Z is an independent and identically distributed noise vector with zero-mean and variance, $\sigma_n^2 = N_0/2$ Gaussian random variable. Here, N_0 denotes the single-sided noise power spectral density. The input symbols, X take values from $\{x_1, x_2, \cdots, x_m\}$ according to the priori PMF given by (1). The AWGN channel can be described by its conditional distribution, $p_{Y|X}(y|x_m)$ as [3]:

$$p_{Y|X}(y|x_m) = \frac{1}{\sqrt{\pi N_0}} \mathrm{e}^{-\frac{|y-x_m|^2}{N_0}}. \tag{2}$$

The MAP detector is thus given by [3]:

$$\hat{m} = \underset{1\leq m\leq M}{\arg\max} \left[p_X(x_m)\, p_{Y|X}(y|x_m)\right]. \tag{3}$$

Consequently, using (1) and (2), the MAP detector in (3) can be evaluated as:

$$\hat{m} = \underset{1\leq m\leq M}{\arg\max} \left[yx_m - \frac{1}{2}(1+N_0\lambda)|x_m|^2\right]. \tag{4}$$

The full derivation of (4) is provided in Appendix B. The decision region, D_m for all $1 \leq m \leq M$ and $1 \leq m' \leq M$ where $m' \neq m$ is given as:

$$D_m = \left\{y(x_m - x_{m'}) > \frac{1}{2}(1+N_0\lambda)\left(|x_m|^2 - |x_{m'}|^2\right)\right\}. \tag{5}$$

Note that from (5), there are at most $M-1$ threshold points, r_{th} where $D_m = D_{m+1}$. In the following sections, the error performance analysis of PS using the MAP detector rule given by (4) is presented. In Section III, the error performance analysis in an AWGN channel condition is presented followed by fading channel conditions in Section IV.

III. ERROR PERFORMANCE IN AWGN CHANNEL

The symbol error probability of the detection scheme is determined by accumulating the product of the priori distribution and the probability of error that occurs when the received symbol is not in the D_m given x_m is transmitted. This can be written as:

$$P_{\mathrm{s}} = \sum_{m=1}^{M} p_X(x_m) \sum_{\substack{1\leq m'\leq M \\ m'\neq m}} \int_{D_{m'}} p_{Y|X}(y|x_m)\,\mathrm{d}y. \tag{6}$$

In the following subsections, the error probability expression is formulated for 4-PAM, which will be used as an example. Then a general SER expression of M-PAM for an arbitrary amplitude level M is derived.

A. Error Probability of 4-PAM

The signalling diagram of 4-PAM with amplitude levels of $x_m = \{\pm 1, \pm 3\}\sqrt{E_{\mathrm{s}}/\xi_{\mathrm{av}}}$ is shown in Fig. 1. Here, E_{s} is the symbol energy while the average symbol energy is denoted by ξ_{av}. For the 4-PAM scheme, the decision boundaries are

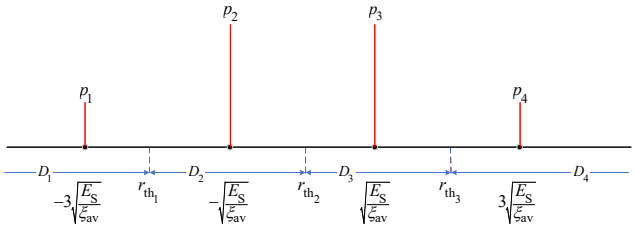

FIGURE 1. PS-4-PAM with symmetrical PMF, decision boundaries and thresholds

determined using (5) as:

$$D_1 = \left\{y < -2(1+N_0\lambda)\sqrt{\frac{E_{\mathrm{s}}}{\xi_{\mathrm{av}}}}\right\} \tag{7a}$$

$$D_2 = \left\{-2(1+N_0\lambda)\sqrt{\frac{E_{\mathrm{s}}}{\xi_{\mathrm{av}}}} < y < 0\right\} \tag{7b}$$

$$D_3 = \left\{0 < y < 2(1+N_0\lambda)\sqrt{\frac{E_{\mathrm{s}}}{\xi_{\mathrm{av}}}}\right\} \tag{7c}$$

$$D_4 = \left\{y > 2(1+N_0\lambda)\sqrt{\frac{E_{\mathrm{s}}}{\xi_{\mathrm{av}}}}\right\}. \tag{7d}$$

Thus, the decision thresholds are $r_{\mathrm{th}_m} = (-2,\ 0,\ 2) \times (1+N_0\lambda)\sqrt{E_{\mathrm{s}}/\xi_{\mathrm{av}}}$ for $m = 1, 2, 3$. Generally, the threshold points of M-PAM can be induced as:

$$r_{\mathrm{th}_m} = (2m-M)(1+N_0\lambda)\sqrt{\frac{E_{\mathrm{s}}}{\xi_{\mathrm{av}}}}. \tag{8}$$

Note that unlike the uniform distribution symbols, the MAP threshold points depend on the noise level and the shaping rate parameter, λ. This is further illustrated in Fig. 2 considering the normalised third threshold point, $\overline{r}_{\mathrm{th}_3} = r_{\mathrm{th}_3}/\sqrt{E_{\mathrm{s}}/\xi_{\mathrm{av}}}$ at different SNR per symbol (E_{s}/N_0) conditions. For equiprobable symbols where $\lambda = 0$, $\overline{r}_{\mathrm{th}_3} = 2$. As λ increases, the threshold point increases and moves to the outer constellation point. The increase is higher in noisy channel ($E_{\mathrm{s}}/N_0 = 10$ dB) compared to a channel with less noise ($E_{\mathrm{s}}/N_0 = 16$ dB).

Taking advantage of the symmetry in amplitude and using (6), the error probability can therefore be evaluated as shown in (9). In this analysis, an error detection has occurred if a symbol m is transmitted but has been detected in $D_{m'}$ region when it should be in region D_m. This is mathematically described in (6). For example, the first term in (9a) describes the case for when $m = 1$ $\left(x = -3\sqrt{\frac{E_{\mathrm{s}}}{\xi_{\mathrm{av}}}}\right)$ is transmitted. For correct detection, it should be received in region D_1. However, if it is received in region $D_{m'}$ for $m' \neq m$ (i.e. m' = 2, 3, 4) then error is detected. Consequently, the range

$$P_{\mathrm{s}} = 2p_1\left[\int_{r_{\mathrm{th}_1}}^{\infty} p\left(y|x=-3\sqrt{\frac{E_{\mathrm{s}}}{\xi_{\mathrm{av}}}}\right)\mathrm{d}y\right] + 2p_2\left[\int_{-\infty}^{r_{\mathrm{th}_1}} p\left(y|x=-\sqrt{\frac{E_{\mathrm{s}}}{\xi_{\mathrm{av}}}}\right)\mathrm{d}y + \int_{r_{\mathrm{th}_2}}^{\infty} p\left(y|x=-\sqrt{\frac{E_{\mathrm{s}}}{\xi_{\mathrm{av}}}}\right)\mathrm{d}y\right] \tag{9a}$$

$$= 2p_1 Q\left(\frac{r_{\mathrm{th}_1} + 3\sqrt{\frac{E_{\mathrm{s}}}{\xi_{\mathrm{av}}}}}{\sqrt{\frac{N_0}{2}}}\right) + 2p_2 Q\left(\frac{-r_{\mathrm{th}_1} - \sqrt{\frac{E_{\mathrm{s}}}{\xi_{\mathrm{av}}}}}{\sqrt{\frac{N_0}{2}}}\right) + 2p_2 Q\left(\frac{r_{\mathrm{th}_2} + \sqrt{\frac{E_{\mathrm{s}}}{\xi_{\mathrm{av}}}}}{\sqrt{\frac{N_0}{2}}}\right) \tag{9b}$$

$$= 2p_1 Q\left((1-2N_0\lambda)\sqrt{\frac{2}{\xi_{\mathrm{av}}}\frac{E_{\mathrm{s}}}{N_0}}\right) + 2p_2 Q\left((1+2N_0\lambda)\sqrt{\frac{2}{\xi_{\mathrm{av}}}\frac{E_{\mathrm{s}}}{N_0}}\right) + 2p_2 Q\left(\sqrt{\frac{2}{\xi_{\mathrm{av}}}\frac{E_{\mathrm{s}}}{N_0}}\right) \tag{9c}$$

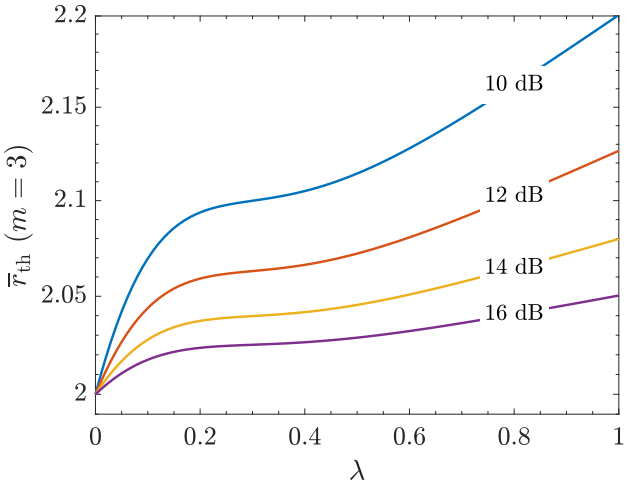

FIGURE 2. The effect of rate parameter, λ and SNR per symbol (E_{s}/N_0) on the normalised third decision point, $\overline{r}_{\mathrm{th}_3}$ of PS-4-PAM

of threshold for erroneous detection is $[r_{\mathrm{th}_1}, \infty)$. Using the fact that $p_2 = p_3$, as shown in Fig. 1, p_2 in the second term of (9c) is replaced by p_3 and (9c) is reformulated in a summation form as follows:

$$P_{\mathrm{s}} = 2\sum_{m=1}^{3} p_m Q\left(\left(1+(2m-4)\,N_0\lambda\right)\sqrt{2\epsilon\frac{E_{\mathrm{s}}}{N_0}}\right). \tag{10}$$

Here, $Q(\cdot)$ denotes the Gaussian Q-function and $\epsilon \triangleq 1/\xi_{\mathrm{av}}$.

B. General Symbol Error Probability Expression of PS-PAM

From the decision boundary expressions in (7), (8), and the SER of 4-PAM in (10), regular patterns can be drawn for general M-PAM signal. This general form of symbol error performance of PS-M-PAM is given as:

$$P_{\mathrm{s}} = 2\sum_{m=1}^{M-1} p_m Q\left(\left(1+(2m-M)\,N_0\lambda\right)\sqrt{2\epsilon\frac{E_{\mathrm{s}}}{N_0}}\right). \tag{11}$$

Note that for equiprobable symbols, $\lambda = 0$ and $p_m = 1/M$ for all m and (11) reduces to the error probability of a conventional uniform M-PAM.

To illustrate the impact of λ on SER given in (11), the SER of PS-16-PAM is shown in Fig. 3 for different λ values. The PS-16-PAM symbols are generated with entropy rates, H = {3, 3.2, 3.6, 3.92} bit/symbol using λ = {0.0331, 0.0250, 0.0132, 0.0047}. The SER of uniform 16-PAM (H = 4 bit/symbol) is also shown for comparison. The result shows that PS achieves better energy efficiency and the gain increases as the λ increases. However, it comes at the cost of reduced net information rate: as λ increases, H decreases. Thus, to maximise the PS gain with optimum entropy level, the knowledge of the channel SNR response of the system is required, from which optimum PMF and thus the entropy is determined by the choice of optimum λ. This optimisation process is realised by minimising the gap between the entropy of symbols to the pre-estimated channel capacity. An experimental study that demonstrates how PS achieves near channel capacity transmission is presented in [15], [17].

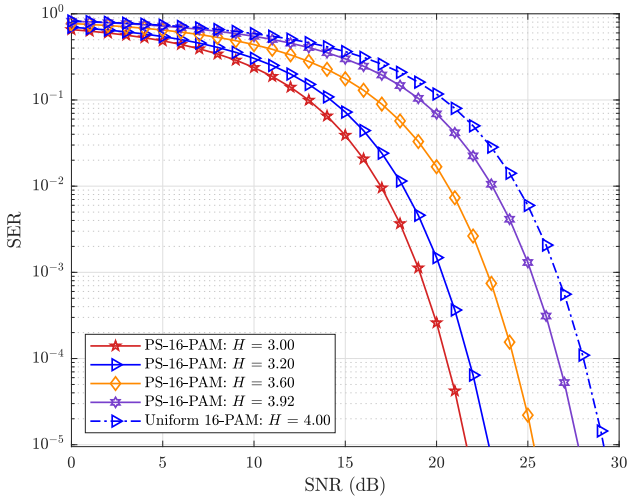

FIGURE 3. Error performance of PS-16-PAM at different entropy levels and uniform 16-PAM

To evaluate the PS error performance independent of a choice of rate parameter, comparison at equal net entropy rates is crucial. To achieve this, a comparison of the SER performance at equal net entropy rates is carried out by using PS-M-PAM symbols against uniform symbols of lower order. The results are shown in Fig. 4 and have been validated with Monte Carlo simulations. The net entropy rates considered are H = 2 bit/symbol (PS-8-PAM and uniform 4-PAM), H = 3 bit/symbol (PS-16-PAM and uniform 8-PAM), and

This article has been accepted for publication in IEEE Open Journal of the Communications Society. This is the author's version which has not been fully edited and content may change prior to final publication. Citation information: DOI 10.1109/OJCOMS.2023.3278972

H = 4 bit/symbol (PS-32-PAM and uniform 16-PAM). As PS has lower H at the same modulation order, higher orders (e.g., $2M$) will be used compared to uniform distribution, which uses M. In all cases, PS has better SER performance than the uniform signal with 1.13 dB, 1.37 dB, 1.43 dB SNR gains at SER = 10^{-3} for H = {2, 3, 4} bit/symbol, respectively. This validates that the SNR gain is not necessarily associated with the entropy reduction. In fact, at equal entropy rates, PS approaches the ultimate 1.53 dB shaping gain. Higher SNR gain can be obtained by using PS-QAM which uses two orthogonal PS-PAM constellations. Generally, irrespective of the SER, a shaping gain can be

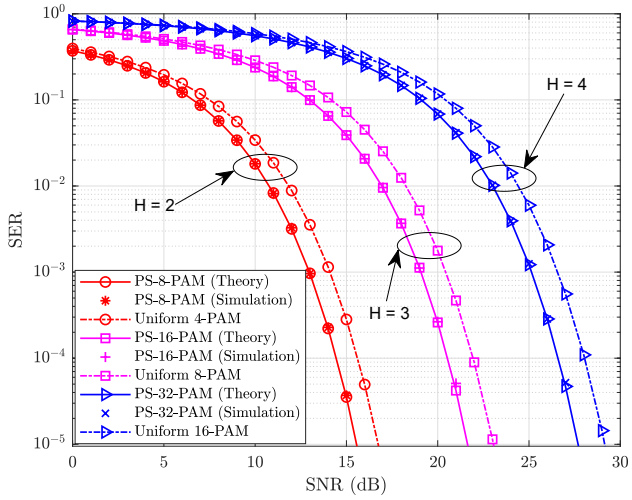

FIGURE 4. Error performance of PS and uniformly distributed PAM for different modulation orders at equal net entropy rates under AWGN channel condition

found by evaluating λ which gives equal entropy, H so that the entropy of the PS, $H_{\text{PS}} = \log_2 M$ and using this λ to evaluate the average symbol energy of PS symbols. Fig 5 shows the shaping gain for increasing entropy values relative to the ultimate shaping gain $\pi e/6$ = 1.5329 dB. The gain increases with entropy until it approaches the ultimate gain asymptotically, as shown in the inset figure.

C. Symbol Error Probability of PS-QAM

The error probability of M-QAM can be determined from the error probability of $\sqrt{M}$-PAM with half the total energy as [3]:

$$P_{\text{s}|M-\text{QAM}} = 1 - \left[1 - P_{\text{s}\left|\sqrt{M}-\text{PAM}\right.}^{E_{\text{s}}/2}\right]^2. \tag{12}$$

Using (12) and the half energy form SER of PS-M-PAM given by (11), the SER of PS-M-QAM is obtained as:

$$P_{\text{s}} = 4\sum_{m=1}^{\sqrt{M}-1} p_m Q\left(\sqrt{\Omega_m \frac{E_{\text{s}}}{N_0}}\right) - 4\left[\sum_{m=1}^{\sqrt{M}-1} p_m Q\left(\sqrt{\Omega_m \frac{E_{\text{s}}}{N_0}}\right)\right]^2 \tag{13}$$

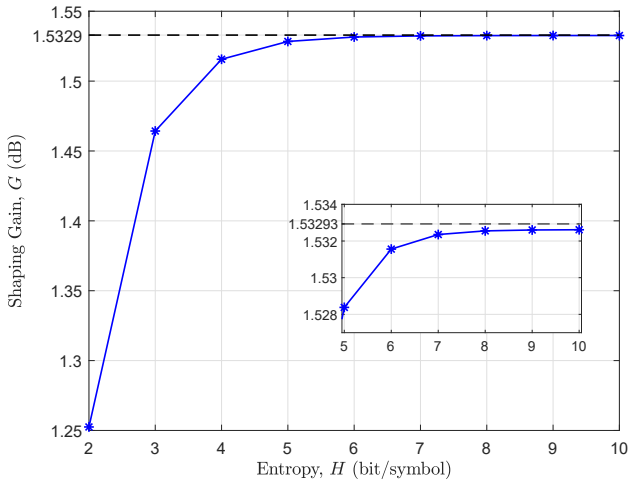

FIGURE 5. Shaping gain for different entropy values. The inset figure shows how the shaping gain approaches the ultimate gain. Dashed black lines show the ultimate shaping gain.

where,

$$\Omega_m = \left(1 + \left(2m - \sqrt{M}\right) N_0 \lambda\right)^2 \epsilon. \tag{14}$$

For PS-4-QAM, all constellation points are in an equal constellation ring with same probabilities. Hence, $\lambda = 0$, $\epsilon = 1$, and $\Omega_m = 1$. Consequently, (13) reduces to:

$$P_{\text{s}} = 2Q\left(\sqrt{\frac{E_{\text{s}}}{N_0}}\right) - Q^2\left(\sqrt{\frac{E_{\text{s}}}{N_0}}\right), \tag{15}$$

which is the same as the symbol error probability of uniformly distributed 4-QAM.

The SER of PS-QAM given by (13) corroborated with Monte Carlo simulation is shown in Fig. 6. For comparison, the SER of the conventional uniformly distributed QAM is also included. In this illustration, PS-M-QAM symbols with M = {16, 64, 256} are generated with entropy, H = {3.6, 5.4, 7.2} bit/symbol using rate parameter, λ = {0.1353, 0.0408, 0.0119}, respectively. The entropy of PS-M-QAM is thus set to be $0.9 \times \log_2 M$ of uniform counterparts. The performance improvement from PS over the uniformly distributed symbols is evident from the result. For all modulation orders shown and ranges of SNR, the PS outperforms uniform distribution. For instance, at SER = 10^{-3}, about 2.12 dB, 2.89 dB, 3.45 dB SNR improvement is obtained from PS-16-QAM, PS-64-QAM, and PS-256-QAM over the corresponding uniform QAM symbols, respectively. Note that the amount of SNR improvement depends on the rate parameter, λ for each modulation order, M.

The SER performance comparison is also repeated at equal net entropy rates by using PS-M-QAM symbols against uniform symbols of lower order ($M/4$-QAM) and presented in Fig. 7. Entropy rates, H = 4 bit/symbol (PS-64-QAM and uniform 16-QAM), H = 6 bit/symbol (PS-256-QAM and uniform 64-QAM), and H = 8 bit/symbol (PS-1024-QAM and uniform 256-QAM) are considered. In all cases, PS has better SER performance than the uniform signal

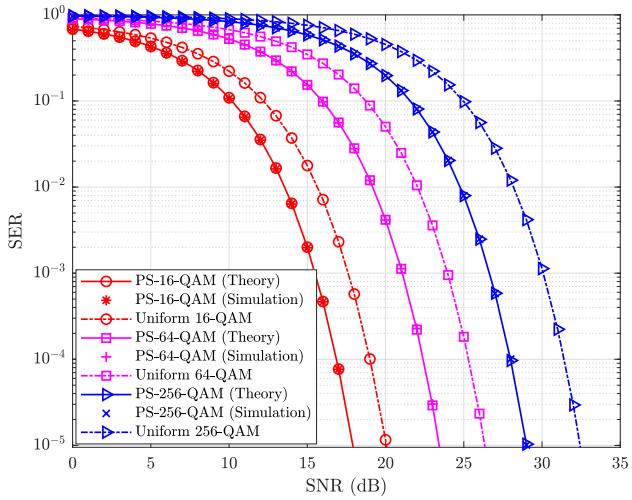

FIGURE 6. Error performance of PS and uniformly distributed QAM for different modulation orders under AWGN channel condition

with SNR gains of 1.16 dB, 1.41 dB, and 1.52 dB for $H = \{4, 6, 8\}$ bit/symbol, respectively, at SER = 10^{-3}. These shaping gains are higher than PS-PAM and achieve the ultimate shaping gain.

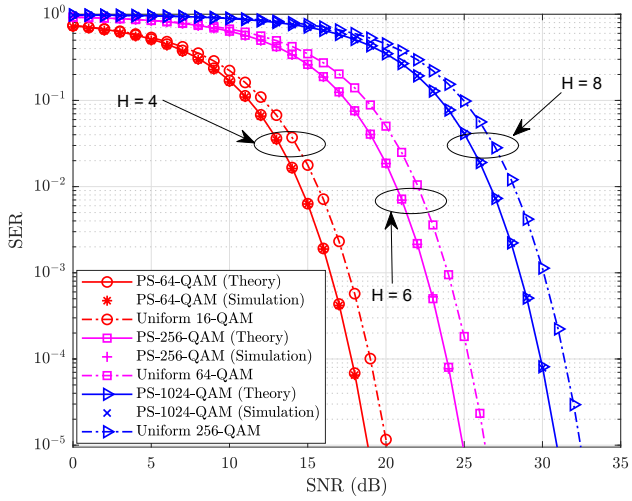

FIGURE 7. Error performance of PS and uniformly distributed QAM at the same net entropy values

IV. ERROR PERFORMANCE IN FADING CHANNELS

In a fading wireless channel, the received instantaneous signal power is scaled by $|h|^2$, where h, the channel coefficient, is a random variable. Thus, the instantaneous SNR per symbol is defined as $\gamma = |h|^2 E_\mathrm{s}/N_0$, and the average SNR per symbol becomes $\overline{\gamma} = |h|^2 E_\mathrm{s}/N_0$. Due to the impact of fading on the received signal amplitude, the decision threshold of M-PAM given in (8) for noise-limited condition will now change to the generalised form given by:

$$r_{\mathrm{th}_m} = (2m - M)\left(|h|^2 + N_0\lambda\right)\frac{1}{h}\sqrt{\frac{E_\mathrm{s}}{\xi_\mathrm{av}}}. \qquad (16)$$

The effect of h and λ on the normalised third decision threshold point, $\overline{r}_{\mathrm{th}_3}$ is demonstrated in Fig. 8. For this instance, SNR = 10 dB is considered. For equiprobable case

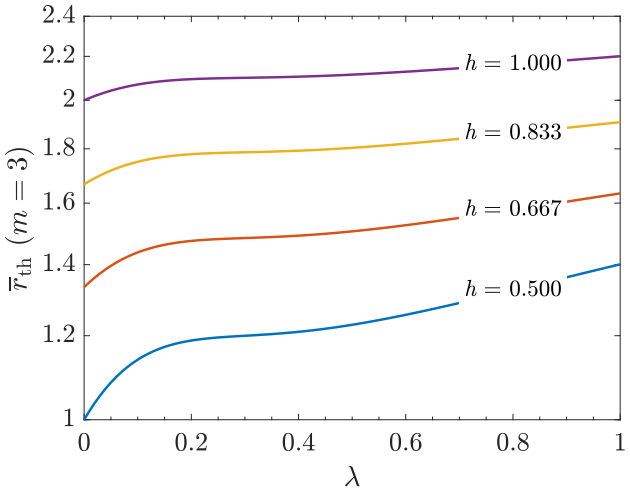

FIGURE 8. The effect of rate parameter, λ and SNR per symbol, E_s/N_0 on the normalised third decision point, $\overline{r}_{\mathrm{th}_3}$ of PS-4-PAM

($\lambda = 0$), and strong attenuation ($h = 0.5$), the threshold is $\overline{r}_{\mathrm{th}_3} = 1$ as against $\overline{r}_{\mathrm{th}_3} = 2$ with $h = 1$. This figure shows that the threshold is no longer fixed but varies with h for any given λ and N_0. In noise-limited case, this depends on the SNR and λ as it was shown in Fig. 2.

The average symbol error probability in the a fading channel then becomes [2]:

$$P_{\mathrm{s|Fading}} = \int_0^\infty P_\mathrm{s}(\gamma)\, p_\gamma(\gamma)\, \mathrm{d}\gamma, \qquad (17)$$

where $p_\gamma(\gamma)$ is a probability density function (PDF) of the instantaneous SNR which depends on the nature of the fading channel. $P_\mathrm{s}(\gamma)$ is evaluated by the SER expression defined in (6) and takes into account the impact of fading on decision thresholds given by (16). However, this leads to an expression which is not tractable. Therefore, in the following subsections, we present a suboptimum tractable SER of Rayleigh and log-normal fading channel conditions with suboptimum decision threshold that is based on (8). It should be noted that the analysis can be easily extended to other fading models.

A. Log-normal Fading Channel

The average symbol error probability in the presence of log-normal fading can be evaluated using (17). The PDF of log-normal fading, $p_\gamma(\gamma)$ is given by [25]:

$$p_\gamma(\gamma) = \frac{1}{\sqrt{2\pi\sigma_I^2}}\frac{1}{\gamma}\exp\left(-\frac{\left(\ln(\gamma/\gamma_0) - \mu\right)^2}{2\sigma_I^2}\right), \quad \gamma \geq 0 \qquad (18)$$

where $\mu = -\sigma_I^2/2$ and σ_γ are the mean and standard deviation of $\ln I$, respectively. From (13) and (18), the SER of PS-M-QAM in log-normal fading channel can be

evaluated, using a Gauss-Hermite quadrature integration [26, equation 25.4.46], as:

$$P_{\rm s} \approx \frac{4}{\sqrt{\pi}} \sum_{n=1}^{N} w_n \sum_{m=1}^{\sqrt{M}-1} p_m Q\left(\Gamma_n \sqrt{\Omega_m \overline{\gamma}}\right) - \frac{4}{\sqrt{\pi}} \sum_{n=1}^{N} w_n \left(\sum_{m=1}^{\sqrt{M}-1} p_m Q\left(\Gamma_n \sqrt{\Omega_m \overline{\gamma}}\right) \right)^2 \quad (19)$$

where,

$$\Gamma_n = I_0 \exp\left(\nu_n \sqrt{2\sigma_I^2} - \sigma_I^2/2\right). \quad (20)$$

Here, $\{\nu_n\}$ and $\{w_n\}$ denote the zeros and weights of the $N^{\rm th}$-order Hermite polynomial with $n = 1, 2, \cdots, N$, respectively. The accuracy of (19) depends on the order of the Hermite polynomial.

The SER performance comparison between PS-QAM in log-normal fading channel (expression (19)), validated with Monte Carlo simulation, and the corresponding uniformly distributed symbols is shown in Fig. 9. For this figure, the fading variance, $\sigma_I^2 = 0.1$ and Hermite polynomial order, $N = 20$, which gives effective approximation to a numerical integration, are considered. Using similar input rates as in the AWGN case, the PS-M-QAM symbols with entropy, H = {3.6, 5.4, 7.2} bit/symbol are generated for M = {16, 64, 256} respectively. The result demonstrates performance improvement from PS compared to the uniform distribution. At SER $= 10^{-3}$, for instance, PS-16-QAM, PS-64-QAM, and PS-256-QAM yield SNR gains of about 2.02 dB, 2.83 dB, 3.40 dB compared to the uniformly distributed QAM symbols, respectively. At the same SER and $\sigma_I^2 = 0.1$, the fading penalty (which quantifies the additional SNR required due to fading at the same BER as the noise-limited case) is about 4.5 dB for both schemes. These results reveal that PS can efficiently improve system performance in a log-normal fading channel as well.

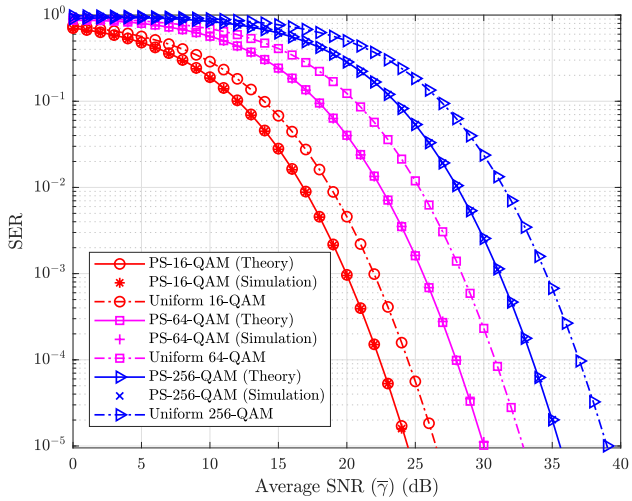

FIGURE 9. Error performance of PS and uniformly distributed QAM for different modulation orders in log-normal fading channel with $\sigma_I^2 = 0.1$

The SER performance comparison is repeated at equal net entropy rates by using entropy rates H = {4, 6, 8} bit/symbol which are used in the AWGN case. The result is presented in Fig. 10. In all cases, PS QAM provides SNR gains of 0.98 dB, 1.33 dB, and 1.47 dB for H = {4, 6, 8} bit/symbol, respectively, at SER = 10^{-3}. However, the SNR gains are lower than the respective AWGN cases. Overall, the

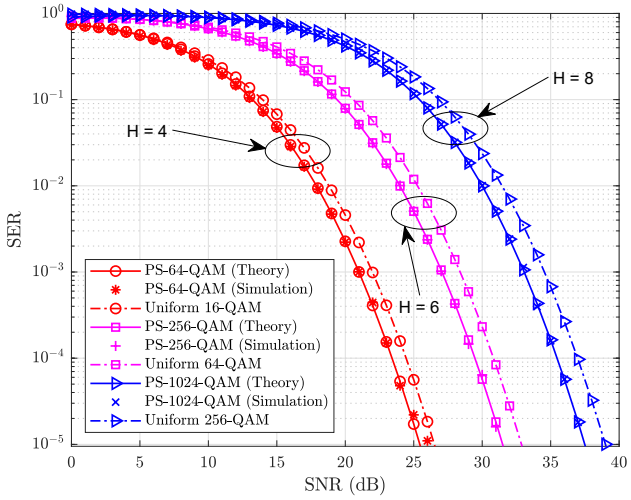

FIGURE 10. Error performance of PS and uniformly distributed QAM at equal net entropy values in log-normal fading channel with $\sigma_I^2 = 0.1$

performance of PS in terms of the SNR gain across different fading variances is evaluated. Here, the SNR gain refers to the improvement in SNR achieved by using PS-based QAM instead of uniformly distributed QAM to achieve a specific BER. The results indicate that the performance of PS is superior to that of the uniform signal in all cases. Figure 11 presents the SNR gain required to achieve a SER of 10^{-3}. The result shows that the highest gain is

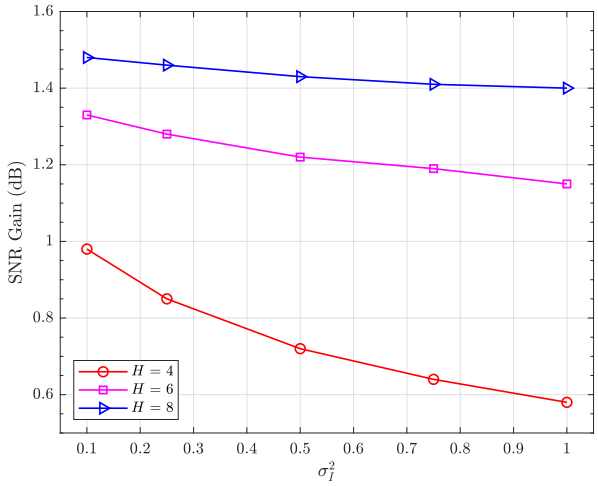

FIGURE 11. The amount of SNR gain from using PS over uniformly distributed QAM at equal net entropy values and SER = 10^{-3} in log-normal fading channel with different σ_I^2

achieved at H = 8 bit/symbol, and despite the increase in

$$P_{\mathrm{s}} \approx 2\sum_{m=1}^{\sqrt{M}-1} p_m\left(1-\sqrt{\frac{\Omega_m\overline{\gamma}}{2+\Omega_m\overline{\gamma}}}\right) - \sum_{m=1}^{\sqrt{M}-1} p_m^2\left(1-\sqrt{\frac{\Omega_m\overline{\gamma}}{2+\Omega_m\overline{\gamma}}}\left(\frac{4}{\pi}\tan^{-1}\left(\sqrt{\frac{2+\Omega_m\overline{\gamma}}{\Omega_m\overline{\gamma}}}\right)\right)\right) - \sum_{j=1}^{\sqrt{M}-1}\sum_{i=1}^{j-1} p_j p_i\left[2-\frac{4}{\pi}\left(\sqrt{\frac{\Omega_i\overline{\gamma}}{2+\Omega_i\overline{\gamma}}}\tan^{-1}\left(\sqrt{\frac{2+\Omega_i\overline{\gamma}}{\Omega_i\overline{\gamma}}}\right)+\sqrt{\frac{\Omega_j\overline{\gamma}}{2+\Omega_j\overline{\gamma}}}\tan^{-1}\left(\sqrt{\frac{2+\Omega_j\overline{\gamma}}{\Omega_j\overline{\gamma}}}\right)\right)\right] \quad (22)$$

fading variance, the gain remains fairly consistent. However, the gain is relatively lower for lower entropy, such as H = 4 bit/symbol, and as the fading variance increases, the gain decreases. This corresponds to the result in Fig. 5, which shows that the shaping gain is higher for larger H values and approaches the ultimate gain.

B. Rayleigh Fading Channel

The PDF of the instantaneous SNR for the Rayleigh fading channel is given by [2]:

$$p_\gamma(\gamma) = \frac{1}{\overline{\gamma}}\exp\left(-\frac{\gamma}{\overline{\gamma}}\right), \quad \gamma \geq 0. \quad (21)$$

Using (13) and (21) in (17), the symbol error probability of PS-M-QAM in Rayleigh fading channel is estimated as given in (22).

Figure 12 shows the SER PS-QAM evaluated by (22) and its Monte Carlo simulation validation. To illustrate,

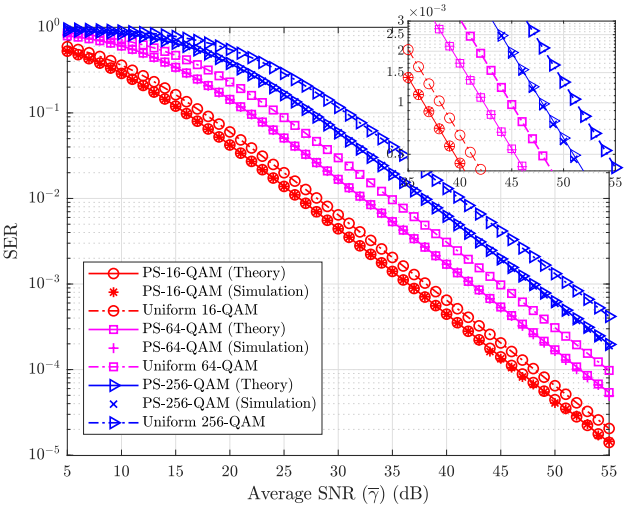

FIGURE 12. Error performance of M-QAM for different modulation orders in Rayleigh fading channel. The inset shows the SER above 35 dB SNR

the PS-M-QAM symbols are generated using entropy, H = {3.6, 5.4, 7.2} bit/symbol for M = {16, 64, 256}, respectively, similar to the AWGN cases. The theoretical uniformly distributed QAM performance under the Rayleigh fading condition is also plotted for comparison. The result demonstrates performance improvement from PS compared to the uniform distribution. At a particular SER of 10^{-3} , for instance, PS-16-QAM, PS-64-QAM, and PS-256-QAM yield SNR gain of about 1.63 dB, 2.59 dB, and 3.27 dB compared to the respective uniform QAM symbols. While at the same SER, the fading penalty is about 21 dB for both schemes. These results demonstrate that PS can effectively improve system performance in a Rayleigh fading wireless channel.

The SER performance comparison at equal net entropy rates is presented in Fig. 13 using entropy rates H = {4, 6, 8} bit/symbol similar to AWGN case. In all

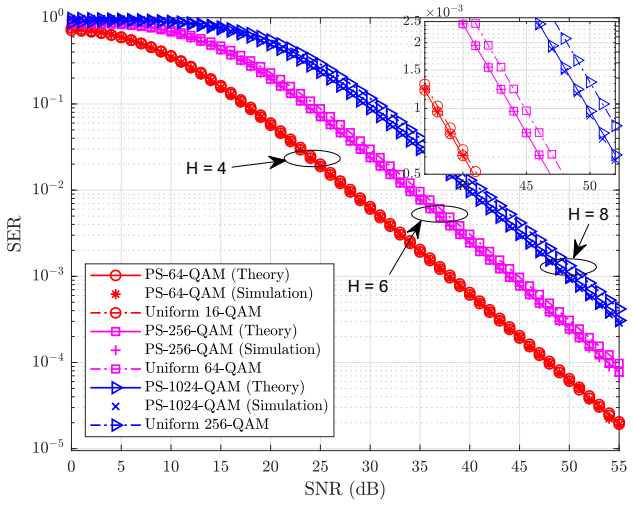

FIGURE 13. Error performance of M-QAM at equal net entropy values in Rayleigh fading channel. The inset shows the SER above 35 dB SNR

entropy values, despite the SNR gains are much lower than the AWGN case, PS has better SER performance than the uniform signal with SNR gains of 0.27 dB, 1.02 dB, and 1.33 dB for H = {4, 6, 8} bit/symbol, respectively, at SER = 10^{-3}.

V. CONCLUSION AND FUTURE WORK

In this work, the symbol error performance analysis of PS with MAP detection scheme has been presented. The analysis is also extended to Rayleigh and log-normal fading channels. The symbol error performance of PS is analysed and closed-form analytical expressions validated with Monte Carlo simulations are provided. This study presents a framework that demonstrates how PS trades energy efficiency (SNR required to achieve a given error performance level) for spectral efficiency and how the design parameters are chosen. These include analysing the effect of the shaping rate parameter, which set the PMF and hence the source entropy and spectral efficiency, on the error performance of

This article has been accepted for publication in IEEE Open Journal of the Communications Society. This is the author's version which has not been fully edited and content may change prior to final publication. Citation information: DOI 10.1109/OJCOMS.2023.3278972

the PS scheme. The result is then compared with the error performance of the traditional uniform distribution. We also compare the SNR gain using a rate parameter which provides an equal entropy between PS and uniformly distributed QAM symbols. Our results show that PS outperforms uniform distribution and it reduces the SNR required to achieve a specific error probability significantly. In AWGN channel, PS-16-QAM, PS-64-QAM, and PS-256-QAM with respective entropy, H = {3.6, 5.4, 7.2} bit/symbol result in SNR gains of 2.12 dB, 2.89 dB, 3.45 dB compared to the uniform 16-QAM, 64-QAM, 256-QAM at SER = 10^{-3}, respectively. Moreover, SNR gains close to the ultimate 1.53 dB shaping gain have been demonstrated by comparing the PS and uniform symbols at equal entropy rates. Using equal entropy, H = {4, 6, 8} bit/symbol between uniform 16-QAM, 64-QAM, and 256-QAM against higher order PS-M-QAM, PS achieve SNR gains of 1.16 dB, 1.41 dB, and 1.52 dB.

The findings of this study have important practical applications in communication systems. The gain in SNR resulting from the use of PS can significantly improve the noise or fading resilience of the system, leading to more reliable and efficient data transmission. This is particularly important in scenarios where power consumption is a critical factor, as PS can enable the design of more energy-efficient wireless communication systems. Alternatively, the increase in SNR can be utilised to improve the achievable information rate without the need to increase the transmitted signal power. This is especially relevant in high-speed applications, where the use of PS can allow for higher data rates and more efficient utilisation of the available bandwidth. Overall, the findings suggest that PS can offer significant benefits for the design and optimisation of communication systems, leading to more robust and efficient communication in various practical applications.

Another possible area of future research would be to investigate the bit error performance of the PS. The BER analysis of PS will be based on the choice of the distribution matcher and FEC. Combining shaping with coding with optimal rates will enhance the SNR gain further.

Appendix A
Maxwell-Boltzmann and Gaussian Distributions

The Maxwell-Boltzmann distribution provides a Gaussian-like distribution for input symbols. It can be shown that the Maxwell-Boltzmann distribution approached the Gaussian distribution depending on the modulation order, M and the rate parameter, λ. Assume a Gaussian distribution given by:

$$f(x) = a \exp\left(-\frac{1}{2}\left(\frac{x-b}{c}\right)^2\right). \tag{23}$$

Since PS symbols are symmetric about $x = 0$, it is possible to use $b = 0$. For (1) to approach the Gaussian distribution in (23), we have:

$$a = \frac{1}{\sum_{j=1}^{M} \mathrm{e}^{-\lambda |x_j|^2}}, \tag{24a}$$

$$c = \frac{1}{\sqrt{2\lambda}}. \tag{24b}$$

Figure 14 shows a PS-based 8-PAM symbol distribution generated with a rate parameter, $\lambda = 0.0435$ and its Gaussian fit, $f(x)$ using $a = 0.2393$, $b = 0$, and $c = 3.3906$.

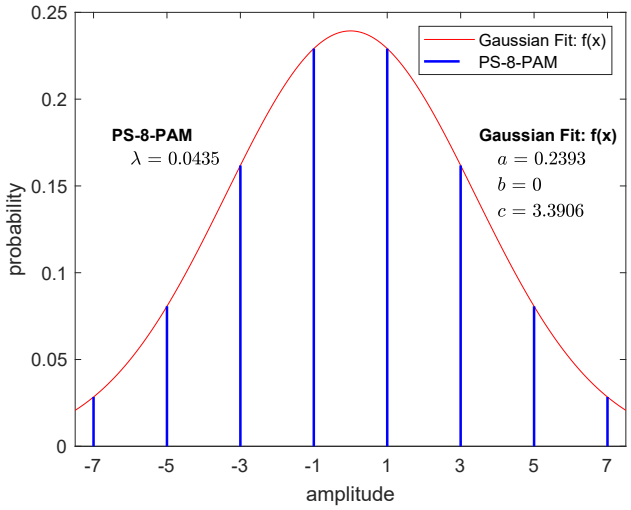

FIGURE 14. PS-8-PAM probability distribution and its Gaussian fit

Appendix B
Derivation of MAP Detector Rule

Substituting (1) and (2) into (3), the full derivation of the MAP detector rule given by (4) is presented as follows:

$$\hat{m} = \underset{1\le m\le M}{\arg\max} \left[\frac{1}{\sum_{j=1}^{M} \mathrm{e}^{-\lambda |x_j|^2}} \mathrm{e}^{-\lambda |x_m|^2} \frac{1}{\sqrt{\pi N_0}} \mathrm{e}^{-\frac{|y-x_m|^2}{N_0}}\right] \tag{25a}$$

$$\overset{(a)}{=} \underset{1\le m\le M}{\arg\max} \left[\mathrm{e}^{-\lambda |x_m|^2} \mathrm{e}^{-\frac{|y-x_m|^2}{N_0}}\right] \tag{25b}$$

$$\overset{(b)}{=} \underset{1\le m\le M}{\arg\max} \left[\ln\left(\mathrm{e}^{-\lambda |x_m|^2} \mathrm{e}^{-\frac{|y-x_m|^2}{N_0}}\right)\right] \tag{25c}$$

$$= \underset{1\le m\le M}{\arg\max} \left[-\lambda |x_m|^2 - \frac{|y-x_m|^2}{N_0}\right] \tag{25d}$$

$$\overset{(c)}{=} \underset{1\le m\le M}{\arg\max} \left[-\frac{N_0}{2}\lambda |x_m|^2 - \frac{1}{2}|y-x_m|^2\right] \tag{25e}$$

$$= \underset{1\le m\le M}{\arg\max} \left[-\frac{N_0}{2}\lambda |x_m|^2 - \frac{1}{2}\left(|y|^2 + |x_m|^2 - 2yx_m\right)\right] \tag{25f}$$

$$\overset{(d)}{=} \underset{1\le m\le M}{\arg\max} \left[yx_m - \frac{1}{2}\left(1 + N_0\lambda\right)|x_m|^2\right]. \tag{25g}$$

In the above simplification, the following assumptions are carried out; (a): positive constants does not change the value and hence are dropped, (b): $\ln(\cdot)$ is an increasing function,

(c): $N_0/2$ is a positive number and multiplying by a positive number does not affect the result, (d): $|y|^2$ is the same for all m and hence it is dropped.

ACKNOWLEDGEMENT

For the purpose of open access, the authors have applied a Creative Commons Attribution (CC BY) licence to any Author Accepted Manuscript version arising from this submission.

REFERENCES

[1] F. Buchali, F. Steiner, G. Böcherer, L. Schmalen, P. Schulte, and W. Idler, "Rate adaptation and reach increase by probabilistically shaped 64-QAM: An experimental demonstration," *Journal of Lightwave Technology*, vol. 34, no. 7, pp. 1599–1609, 2016.

[2] M. K. Simon and M.-S. Alouini, *Digital communication over fading channels*. John Wiley & Sons, 2005, vol. 95.

[3] J. G. Proakis and M. Salehi, *Digital communications*. McGraw-hill New York, 2001, vol. 4.

[4] K. Cho and D. Yoon, "On the general BER expression of one- and two-dimensional amplitude modulations," *IEEE Transactions on Communications*, vol. 50, no. 7, pp. 1074–1080, 2002.

[5] S. B. Slimane and T. Le-Ngoc, "Tight bounds on the error probability of coded modulation schemes in Rayleigh fading channels," *IEEE Transactions on Vehicular Technology*, vol. 44, no. 1, pp. 121–130, 1995.

[6] M. Chiani, D. Dardari, and M. K. Simon, "New exponential bounds and approximations for the computation of error probability in fading channels," *IEEE Transactions on Wireless Communications*, vol. 2, no. 4, pp. 840–845, 2003.

[7] J. Bao, Z. Ma, M. Xiao, Z. Ding, and Z. Zhu, "Performance analysis of uplink SCMA with receiver diversity and randomly deployed users," *IEEE Transactions on Vehicular Technology*, vol. 67, no. 3, pp. 2792–2797, 2017.

[8] F. R. Kschischang and S. Pasupathy, "Optimal nonuniform signaling for Gaussian channels," *IEEE Transactions on Information Theory*, vol. 39, no. 3, pp. 913–929, 1993.

[9] P. Schulte and G. Böcherer, "Constant composition distribution matching," *IEEE Transactions on Information Theory*, vol. 62, no. 1, pp. 430–434, 2015.

[10] U. Wachsmann, R. F. Fischer, and J. B. Huber, "Multilevel codes: Theoretical concepts and practical design rules," *IEEE Transactions on Information Theory*, vol. 45, no. 5, pp. 1361–1391, 1999.

[11] G. Forney and L.-F. Wei, "Multidimensional constellations. I. Introduction, figures of merit, and generalized cross constellations," *IEEE Journal on Selected Areas in Communications*, vol. 7, no. 6, pp. 877–892, 1989.

[12] J. Cho and P. J. Winzer, "Probabilistic constellation shaping for optical fiber communications," *Journal of Lightwave Technology*, vol. 37, no. 6, pp. 1590–1607, 2019.

[13] F. Buchali, G. Böcherer, W. Idler, L. Schmalen, P. Schulte, and F. Steiner, "Experimental demonstration of capacity increase and rate-adaptation by probabilistically shaped 64-QAM," in *2015 European Conference on Optical Communication (ECOC)*. IEEE, 2015, pp. 1–3.

[14] T. Fehenberger, A. Alvarado, G. Böcherer, and N. Hanik, "On probabilistic shaping of quadrature amplitude modulation for the nonlinear fiber channel," *Journal of Lightwave Technology*, vol. 34, no. 21, pp. 5063–5073, 2016.

[15] T. Z. Gutema and W. O. Popoola, "Single LED Gbps visible light communication with probabilistic shaping," in *GLOBECOM 2021-2021 IEEE Global Communications Conference*. IEEE, 2021, pp. 1–6.

[16] X. Hong, C. Fei, G. Zhang, and S. He, "Probabilistically shaped 256-QAM-OFDM transmission in underwater wireless optical communication system," in *2019 Optical Fiber Communications Conference and Exhibition (OFC)*. IEEE, 2019, pp. 1–3.

[17] T. Z. Gutema, H. Haas, and W. O. Popoola, "WDM based 10.8 Gbps visible light communication with probabilistic shaping," *Journal of Lightwave Technology*, vol. 40, no. 15, pp. 5062–5069, 2022.

[18] S. Wang, Z. Lu, W. Li, S. Jia, L. Zhang, M. Qiao, X. Pang, N. Idrees, M. Saqlain, X. Gao *et al.*, "26.8-m THz wireless transmission of probabilistic shaping 16-QAM-OFDM signals," *APL Photonics*, vol. 5, no. 5, p. 056105, 2020.

[19] K. Wang, X. Li, M. Kong, P. Gou, W. Zhou, and J. Yu, "Probabilistically shaped 16QAM signal transmission in a photonics-aided wireless terahertz-wave system," in *Optical Fiber Communication Conference*. Optical Society of America, 2018, pp. M4J–7.

[20] X. Li, J. Yu, L. Zhao, W. Zhou, K. Wang, M. Kong, G.-K. Chang, Y. Zhang, X. Pan, and X. Xin, "132-Gb/s photonics-aided single-carrier wireless terahertz-wave signal transmission at 450GHz enabled by 64QAM modulation and probabilistic shaping," in *Optical Fiber Communication Conference*. Optical Society of America, 2019, pp. M4F–4.

[21] S. Javed, A. Elzanaty, O. Amin, B. Shihada, and M.-S. Alouini, "When Probabilistic Shaping Realizes Improper Signaling for Hardware Distortion Mitigation," *IEEE Transactions on Communications*, vol. 69, no. 8, pp. 5028–5042, 2021.

[22] Y. Yao, K. Xiao, B. Xia, and Q. Gu, "Design and analysis of rotated-QAM based probabilistic shaping scheme for Rayleigh fading channels," *IEEE Transactions on Wireless Communications*, vol. 19, no. 5, pp. 3047–3063, 2020.

[23] J. Ma, J. He, M. Chen, and K. Wu, "Performance enhancement of probabilistically shaped OFDM enabled by precoding technique in an IM-DD system," *Journal of Lightwave Technology*, vol. 37, no. 24, pp. 6063–6071, 2019.

[24] G. Böcherer, F. Steiner, and P. Schulte, "Bandwidth efficient and rate-matched low-density parity-check coded modulation," *IEEE Transactions on communications*, vol. 63, no. 12, pp. 4651–4665, 2015.

[25] M. Safari and M. Uysal, "Relay-assisted free-space optical communication," *IEEE Transactions on Wireless Communications*, vol. 7, no. 12, pp. 5441–5449, 2008.

[26] M. Abramowitz, I. A. Stegun, and R. H. Romer, "Handbook of mathematical functions with formulas, graphs, and mathematical tables," 1988.

Tilahun Zerihun Gutema (Graduate Student Member, IEEE) received his B.Sc. degree in electrical engineering from Addis Ababa University, Addis Ababa, Ethiopia in 2015, and his M.Sc. degree in optics and photonics, from Karlsruhe Institute of Technology, Karlsruhe, Germany, in 2018. He is currently working toward the Ph.D. degree at the University of Edinburgh, U.K. He is also a Marie Curie Early-Stage Researcher. His main research interest includes digital modulation techniques and visible light communication.

Harald Haas (FREng FRSE FIEEE FIET) received the Ph.D. degree from The University of Edinburgh in 2001. He is a Distinguished Professor of Mobile Communications at the University of Strathclyde and the Director of the LiFi Research and Development Centre. He also set-up and co-founded pureLiFi Ltd which it currently serves as Chief Scientific Officer. He has authored over 550 conference and journal papers. Haas' main research interests are in optical wireless communications, hybrid optical wireless and RF communications, spatial modulation, and interference coordination in wireless networks. His team invented spatial modulation. He introduced LiFi to the public at an invited TED Global talk in 2011. LiFi was listed among the 50 best inventions in TIME Magazine in 2011. In 2016, he received the Outstanding Achievement Award from the International Solid State Lighting Alliance. In 2019 he was the recipient of the IEEE Vehicular Society James Evans Avant Garde Award. Haas was elected a Fellow of the Royal Society of Edinburgh (RSE) in 2017. In the same year, he received a Royal Society Wolfson Research Merit Award and was elevated to IEEE Fellow. In 2018 he received a three-year EPSRC Established Career Fellowship extension and was elected Fellow of the IET. Haas was elected Fellow of the Royal Academy of Engineering (FREng) in 2019.

Wasiu O. Popoola (Senior Member, IEEE) is currently a University Reader and Deputy Director of Learning and Teaching with the School of Engineering, University of Edinburgh, Edinburgh, U.K. He has authored or coauthored more than 120 journal articles/conference articles/patent and over seven of those are invited articles. He also co-authored the book Optical Wireless Communications: System and Channel Modeling with MATLAB and many other book chapters. His primary research interests are digital and optical communications, including VLC, FSO, and fiber communications. One of his journal articles ranked No. 2 in terms of the number of full text downloads within IEEE Xplore, in 2008, from the hundreds of articles published by IET Optoelectronics, since 1980. Another article he coauthored with one of his Ph.D. students received the Best Poster Award at the 2016 IEEE ICSAE Conference.

Dr. Popoola is a science communicator appearing in science festivals and on "BBC Radio 5live Science" programme in Oct. 2017. His publications have more 6200 citations and an h-index of 34 on Google Scholar. He is an Associate Editor of the IEEE ACCESS JOURNAL, a Fellow of the Institute of Engineering Technology (FIET), and a Fellow of the Higher Education Academy (FHEA). He was an Invited speaker at various events including the 2016 IEEE Photonics Society Summer Topicals.